

Transverse-momentum resummation for photon pair production at NNLL+NLO

Leandro Cieri

Physik-Institut, Universität Zürich, CH-8057 Zürich, Switzerland

E-mail: lcieri@physik.uzh.ch

Abstract. We are interested in the transverse-momentum (q_T) distribution of a diphoton pair produced in hadron collisions. We resum the logarithmically-enhanced perturbative QCD contributions at small values of q_T up to next-to-next-to-leading logarithmic accuracy. We consistently combine resummation with the known next-to-leading order perturbative result at intermediate and large values of q_T . We include all perturbative terms up to order α_S^2 in our computation which, after integration over q_T , reproduces the known next-to-next-to-leading order result for the diphoton pair production total cross section. A comparison with LHC data is presented. We estimate the perturbative accuracy of the theoretical calculation by performing the corresponding variation of scales. We anticipate that the effect of the transverse momentum resummation is not only to recover the predictivity of the calculation at small q_T , but also to improve substantially the agreement with the experimental data.

1. Introduction

The production of two isolated photons at hadronic colliders is a very relevant process, both from the point of view of testing the Standard Model (SM) predictions [1, 2, 3, 4, 5, 6] as for new physics searches.

Direct or *prompt* photons provide an ideal test to the understanding of pQCD since they constitute a theoretically and experimentally *clean* final state. From the theory side, because they do not have QCD interactions with other final state particles and, from the experimental point of view, because their energies and momenta can be measured with high precision in modern electromagnetic calorimeters.

Diphoton final states have played a crucial role in the recent discovery of a new boson at the LHC [7, 8], whose properties are compatible with those of the SM Higgs. They are also important in many new physics scenarios [9, 10], in particular in the search for extra-dimensions [11] or supersymmetry [12].

We are interested in the process $pp \rightarrow \gamma\gamma X$, and in particular in the transverse-momentum (q_T) spectrum of the diphoton pair. At the lowest-order ($\mathcal{O}(\alpha_S^0)$) the diphoton final state occurs *via* the quark annihilation subprocess $q\bar{q} \rightarrow \gamma\gamma$. The QCD corrections at the first order in the strong coupling α_S involve quark annihilation and a new partonic channel, *via* the subprocess $qg \rightarrow \gamma\gamma q$.

Several fully-differential Monte Carlo codes implement the first order corrections [13, 14, 15, 16]. At the second order in the strong coupling α_S the gg channel starts to contribute, and the large gluon-gluon luminosity makes this channel potentially sizeable.

The matrix elements needed to evaluate the corrections at the second order in the strong coupling α_S , for diphoton production, have been presented in [17, 18, 19, 20], and first put together in a complete and consistent $\mathcal{O}(\alpha_S^2)$ calculation in the $2\gamma\text{NNLO}$ code [21]. The next-order corrections to the *box contribution* (which are part of the N^3LO QCD corrections to diphoton production) were also computed in ref. [14] and found to have a moderate quantitative effect.

The calculation of the q_T spectrum requires the identification of two kinematic regions. In the large- q_T region ($q_T \sim M_{\gamma\gamma}$), where the transverse momentum is of the order of the diphoton invariant mass $M_{\gamma\gamma}$, calculations based on the truncation of the perturbative series at a fixed order in α_S are theoretically justified. In this kinematic region, the QCD radiative corrections are known up to the next-to-leading order (NLO), including the corresponding partonic scattering amplitudes with $X = 2$ partons (at the tree level [18]) and the partonic scattering amplitudes with $X = 1$ parton (up to the one-loop level [19]). In order to have $q_T \neq 0$ for the diphoton pair, at least one additional parton is needed. The transverse momentum spectrum of the diphoton pair has been calculated in fully-differential Monte Carlo codes at LO [13, 14, 15, 16] and at NLO [21, 22, 23]. Recently, first calculations for diphoton production in association with two [24, 25, 26] and three [26] jets at NLO became available.

In the small- q_T region ($q_T \ll M_{\gamma\gamma}$), where the bulk of the diphoton events is produced, the convergence of the fixed-order expansion is spoiled by the presence of large logarithmic terms, $\alpha_S^n \ln^m(M_{\gamma\gamma}^2/q_T^2)$. These logarithmically-enhanced terms have to be resummed to all perturbative orders [27]–[38] in order to obtain reliable predictions. The resummed calculation, valid at small values of q_T , and the fixed-order one at large q_T have then to be consistently matched to obtain a pQCD prediction for the entire range of transverse momenta.

We use the transverse-momentum resummation formalism proposed in Refs. [37, 39, 40] (see also [41] for processes initiated by gg annihilation). The formalism is valid for a generic process in which a high-mass system of non strongly-interacting particles is produced in hadron-hadron collisions. The method has so far been applied to the production of the Standard Model (SM) Higgs boson [39, 40, 42, 43, 44], Higgs boson production in bottom quark annihilation [45], Higgs boson production via gluon fusion in the MSSM [46], single vector bosons at NLL+LO [47] and at NNLL+NLO [48] with leptonic decay [49], WW [50, 51] and ZZ [52] pairs, vector boson pair production at NNLL+NLO [53], slepton pairs [54], DY lepton pairs in polarized collisions [55] and recently we applied it to diphoton production at NNLL+NLO [56].

It is necessary to notice that besides the direct photon contribution from the hard subprocess, photons can also be produced from the fragmentation of QCD partons. Calculate the fragmentation subprocesses requires (the poorly known) non-perturbative information, in the form of parton fragmentation functions of the photon (the complete single- and double-fragmentation contributions are implemented in DIPHOX [13] for diphoton production at the first order in α_S). Moreover, including this contribution could be non trivial at NNLO since we have particles with colour in the final state, and the q_T resummation formalism, at least in its original form ¹, has to be generalized in order to make it possible treat colour particles in the final state. It is important to notice that the effect of the fragmentation contributions is sizeably reduced by the *photon isolation* criteria that are necessarily applied in hadron collider experiments to suppress the very large irreducible background (*e.g.*, photons that are faked by jets or produced by hadron decays). Two such criteria are the so-called “standard” cone isolation and the “smooth” cone isolation proposed by Frixione [57]. The standard cone isolation is easily implemented in experiments, but it only suppresses a fraction of the fragmentation contribution. In the case of the smooth cone isolation, it (formally) eliminates the entire fragmentation contribution. For all of the results presented in this proceeding we rely on the smooth isolation prescription, which,

¹ The formalism is general, as long as the measured final state is composed of non strongly-interacting particles. Transverse-momentum resummation for strongly-interacting final states, such as heavy-quark production, has been developed in Refs. [59, 60].

for the parameters used in the experimental analysis reproduces the standard result within a 1% accuracy [58].

This proceeding is organized as follows. In Sect. 2 we briefly review the resummation formalism of Refs. [37, 39, 40]. In Sect. 3 we present numerical results and we comment on their comparison with the LHC data [6]. We also study the scale dependence of our results with the purpose of estimating the corresponding perturbative uncertainty. In Sect. 4 we summarize our results.

2. The transverse-momentum resummation formalism

We briefly introduce the main points of the transverse-momentum resummation formalism of Refs. [37, 39, 40], referring to the original papers for the full details. The formalism is general, as long as the measured final state is composed of non strongly-interacting particles (transverse-momentum resummation for strongly-interacting final states, such as heavy-quark production, has been developed in Refs. [59, 60]). Here we specialize to the case of diphoton production only for ease of reading. The inclusive hard-scattering process considered is

$$h_1(p_1) + h_2(p_2) \rightarrow \gamma\gamma(M_{\gamma\gamma}, q_T, y) + X, \quad (1)$$

where h_1 and h_2 are the colliding hadrons with momenta p_1 and p_2 , $\gamma\gamma$ is the diphoton pair with invariant mass $M_{\gamma\gamma}$, transverse momentum q_T and rapidity y , and X is an arbitrary and undetected final state.

Using the factorization formula, we can write the corresponding fully differential cross section, in q_T , $M_{\gamma\gamma}$ and y , which we denote for simplicity (since our focus is on the q_T distribution) by $d\sigma_{\gamma\gamma}/dq_T^2$,

$$\frac{d\sigma_{\gamma\gamma}}{dq_T^2}(q_T, M_{\gamma\gamma}, s) = \sum_{a,b} \int_0^1 dx_1 \int_0^1 dx_2 f_{a/h_1}(x_1, \mu_F^2) f_{b/h_2}(x_2, \mu_F^2) \frac{d\hat{\sigma}_{ab}^{\gamma\gamma}}{dq_T^2}(q_T, M_{\gamma\gamma}, y, \hat{s}; \alpha_S, \mu_R^2, \mu_F^2) \quad (2)$$

(up to power-suppressed corrections), where the $f_{a/h}(x, \mu_F^2)$ ($a = q, \bar{q}, g$) are the parton densities of the hadron h at the factorization scale μ_F , $\alpha_S \equiv \alpha_S(\mu_R^2)$, $d\hat{\sigma}_{ab}^{\gamma\gamma}/dq_T^2$ is the pQCD *partonic cross section*, s ($\hat{s} = x_1 x_2 s$) is the square of the hadronic (partonic) centre-of-mass energy, and μ_R is the renormalization scale.

In the large q_T region ($q_T \sim M_{\gamma\gamma}$) the QCD perturbative series is controlled by a small expansion parameter, $\alpha_S(M_{\gamma\gamma})$, and a fixed-order calculation of the partonic cross section is theoretically justified. For these values of transverse momentum, the QCD radiative corrections are known up to next-to-leading order (NLO) [17, 18, 19, 20].

The convergence of the fixed-order perturbative expansion, in the small- q_T region ($q_T \ll M_{\gamma\gamma}$), is spoiled by the presence of powers of large logarithmic terms, $\alpha_S^n \ln^m(M_{\gamma\gamma}^2/q_T^2)$. In order to obtain reliable predictions these terms have to be resummed to all orders.

To apply the transverse momentum resummation, we start by decomposing the partonic cross section as

$$\frac{d\hat{\sigma}_{ab}^{\gamma\gamma}}{dq_T^2} = \frac{d\hat{\sigma}_{\gamma\gamma ab}^{(\text{res.})}}{dq_T^2} + \frac{d\hat{\sigma}_{\gamma\gamma ab}^{(\text{fin.})}}{dq_T^2}. \quad (3)$$

The first term on the right-hand side contains all the logarithmically-enhanced contributions, which have to be resummed to all orders in α_S , while the second term is free of such contributions and can thus be evaluated at fixed order in perturbation theory. Using the Fourier transformation between the conjugate variables q_T and b (b is the impact parameter), the resummed component

$d\hat{\sigma}_{\gamma\gamma ab}^{(\text{res.})}$ can be expressed as

$$\frac{d\hat{\sigma}_{\gamma\gamma ab}^{(\text{res.})}}{dq_T^2}(q_T, M_{\gamma\gamma}, y, \hat{s}; \alpha_S, \mu_R^2, \mu_F^2) = \frac{M_{\gamma\gamma}^2}{\hat{s}} \int_0^\infty db \frac{b}{2} J_0(bq_T) \mathcal{W}_{ab}^{\gamma\gamma}(b, M_{\gamma\gamma}, y, \hat{s}; \alpha_S, \mu_R^2, \mu_F^2), \quad (4)$$

where $J_0(x)$ is the 0th-order Bessel function. The form factor $\mathcal{W}^{\gamma\gamma}$ is best expressed in terms of its *double* Mellin moments $\mathcal{W}_{N_1 N_2}^{\gamma\gamma}$, taken with respect to the variables z_1, z_2 at fixed $M_{\gamma\gamma}$, with

$$z_1 z_2 \equiv z = \frac{M_{\gamma\gamma}^2}{\hat{s}}, \quad \frac{z_1}{z_2} = e^{2y}; \quad (5)$$

the resummation structure of $\mathcal{W}_{N_1 N_2}^{\gamma\gamma}$ can be organized in an exponential form ²

$$\begin{aligned} \mathcal{W}_{N_1 N_2}^{\gamma\gamma}(b, M_{\gamma\gamma}, y; \alpha_S, \mu_R^2, \mu_F^2) &= \mathcal{H}_{N_1 N_2}^{\gamma\gamma}(M_{\gamma\gamma}, \alpha_S; M_{\gamma\gamma}^2/\mu_R^2, M_{\gamma\gamma}^2/\mu_F^2, M_{\gamma\gamma}^2/\mu_{res}^2) \\ &\times \exp\{\mathcal{G}_{N_1 N_2}(\alpha_S, L; M_{\gamma\gamma}^2/\mu_R^2, M_{\gamma\gamma}^2/\mu_{res}^2)\} \quad , \end{aligned} \quad (6)$$

where we have defined the logarithmic expansion parameter $L \equiv \ln(1 + \mu_{res}^2 b^2/b_0^2)$ [39, 42], and $b_0 = 2e^{-\gamma_E}$ ($\gamma_E = 0.5772\dots$ is the Euler number).

The argument of the logarithmic expansion parameter L ensures the unitarity constraint. If we take $b = 0$ which directly implies $L = 0$, it is easy to demonstrate that after inclusion of the finite component (see Eq. (10)), we exactly recover the fixed-order perturbative value of the total cross section upon integration of the q_T distribution over q_T (i.e., the resummed terms give a vanishing contribution upon integration over q_T). In particular we have,

$$\begin{aligned} \int_0^\infty dq_T^2 \frac{d\hat{\sigma}_{\gamma\gamma}^{(\text{res.})}}{dq_T^2}(q_T, M_{\gamma\gamma}, \hat{s}; \alpha_S(\mu_R^2), \mu_R^2, \mu_F^2, \mu_{res}^2) &= \\ \frac{M_{\gamma\gamma}^2}{\hat{s}} \mathcal{H}^{\gamma\gamma}(M_{\gamma\gamma}, \hat{s}, \alpha_S(\mu_R^2); M_{\gamma\gamma}^2/\mu_R^2, M_{\gamma\gamma}^2/\mu_F^2, M_{\gamma\gamma}^2/\mu_{res}^2) \quad . \end{aligned} \quad (7)$$

The scale μ_{res} ($\mu_{res} \sim M_{\gamma\gamma}$), which appears on the right-hand side of Eqs. (6) and (7), is the resummation scale [39]. The form factor $\mathcal{W}_{N_1 N_2}^{\gamma\gamma}$ (i.e., the product $\mathcal{H}_{N_1 N_2}^{\gamma\gamma} \times \exp\{\mathcal{G}_{N_1 N_2}\}$) does not depend on μ_{res} when evaluated to all perturbative orders. Its explicit dependence on μ_{res} appears when $\mathcal{W}_{N_1 N_2}^{\gamma\gamma}$ is computed by truncation of the resummed expression at some level of logarithmic accuracy (see Eq. (8) below). We can use variations of μ_{res} around $M_{\gamma\gamma}$ in order to estimate the size of yet uncalculated higher-order logarithmic contributions.

The form factor $\exp\{\mathcal{G}_{N_1 N_2}\}$ is universal³ and contains all the terms that order-by-order in α_S are logarithmically divergent as $b \rightarrow \infty$ (or, equivalently, $q_T \rightarrow 0$). The resummed logarithmic expansion of the exponent $\mathcal{G}_{N_1 N_2}$ is defined as follows:

$$\begin{aligned} \mathcal{G}_{N_1 N_2}(\alpha_S, L; M_{\gamma\gamma}^2/\mu_R^2, M_{\gamma\gamma}^2/\mu_{res}^2) &= L g^{(1)}(\alpha_S L) + g_{N_1 N_2}^{(2)}(\alpha_S L; M_{\gamma\gamma}^2/\mu_R^2, M_{\gamma\gamma}^2/\mu_{res}^2) \\ &+ \frac{\alpha_S}{\pi} g_{N_1 N_2}^{(3)}(\alpha_S L, M_{\gamma\gamma}^2/\mu_R^2, M_{\gamma\gamma}^2/\mu_{res}^2) + \dots \end{aligned} \quad (8)$$

where the term $L g^{(1)}$ collects the leading logarithmic (LL) $\mathcal{O}(\alpha_s^{p+n} L^{n+1})$ contributions, the function $g_{N_1 N_2}^{(2)}$ includes the next-to-leading leading logarithmic (NLL) $\mathcal{O}(\alpha_s^{p+n} L^n)$ contributions

² For the sake of simplicity we consider here only the case of the diagonal terms in the flavour space of the partonic indices a, b . For a detailed discussion, we refer to Ref. [39, 40].

³ The form factor does not depend on the final state; all the hard-scattering processes initiated by $q\bar{q}$ (gg) annihilation have the same form factor.

[32], $g_{N_1 N_2}^{(3)}$ controls the NNLL $\mathcal{O}(\alpha_s^{p+n} L^{n-1})$ terms [33, 34, 61, 62] and so forth; p is the number of powers of α_s in the LO (Born) process. In Eq. (8), $\alpha_s L$ is formally of order 1, so there is an explicit $\mathcal{O}(\alpha_s)$ suppression between different logarithmic orders. The explicit form of the functions $g^{(1)}$, $g_{N_1 N_2}^{(2)}$ and $g_{N_1 N_2}^{(3)}$ can be found in Ref. [39]. The process dependent function $\mathcal{H}_{N_1 N_2}^\gamma$ does not depend on the impact parameter b and it includes all the perturbative terms that behave as constants as $b \rightarrow \infty$. It can thus be expanded in powers of α_s :

$$\mathcal{H}_{N_1 N_2}^\gamma(M_{\gamma\gamma}, \alpha_s; M_{\gamma\gamma}^2/\mu_R^2, M_{\gamma\gamma}^2/\mu_F^2, M_{\gamma\gamma}^2/\mu_{res}^2) = \sigma_{\gamma\gamma}^{(0)}(\alpha_s, M_{\gamma\gamma}) \left[1 + \frac{\alpha_s}{\pi} \mathcal{H}_{N_1 N_2}^{\gamma\gamma(1)}(M_{\gamma\gamma}^2/\mu_F^2, M_{\gamma\gamma}^2/\mu_{res}^2) + \left(\frac{\alpha_s}{\pi} \right)^2 \mathcal{H}_{N_1 N_2}^{\gamma\gamma(2)}(M_{\gamma\gamma}^2/\mu_R^2, M_{\gamma\gamma}^2/\mu_F^2, M_{\gamma\gamma}^2/\mu_{res}^2) + \dots \right], \quad (9)$$

where $\sigma_{\gamma\gamma}^{(0)}$ is the partonic cross section at the Born level. Since the formalism applies to non strongly-interacting final states, in general the Born cross-section can only correspond to a $q\bar{q}$ or gg initial state. In the specific case of the diphoton production, both channels contribute, but at different orders in α_s : the $q\bar{q}$ subprocess initiates as a pure QED process ($\mathcal{O}(\alpha_s)^0$), while the gg one requires a fermion loop, starting at $\mathcal{O}(\alpha_s)^2$.

In the present work, we keep contributions up to a uniform order in α_s (and all orders in $\alpha_s L$), namely up to $\alpha_s^n L^{n-1}$. For the $q\bar{q}$ channel, this requires the inclusion of the \mathcal{H} coefficients of Eq. (9) up to order 2: the first-order coefficients $\mathcal{H}_{N_1 N_2}^{\gamma\gamma(1)}$ are known since a long time [61], while the second-order coefficients $\mathcal{H}_{N_1 N_2}^{\gamma\gamma(2)}$ were computed only relatively recently [21, 38]. For the gg channel, it is sufficient to include the leading \mathcal{H} contribution (that is, the Born cross-section) and the appropriate \mathcal{G} in the exponential of Eq. (8). Since it does not require any additional numerical effort, we decided, in all the plots presented in the proceeding, to include all the terms up to $g_{N_1 N_2}^{(3)}$ in the exponential \mathcal{G} factor also for this channel. In this way, we technically include some terms which are of higher order in α_s with respect to those in the $q\bar{q}$ channel; however we checked that those terms result in a negligible numerical effect (at 1% accuracy), that is, the difference produced by including the higher order terms is within the error bands obtained by the scale variations, which verifies the stability of the calculation.

The finite component in the Eq. (3) is the remaining ingredient of the transverse-momentum cross section. Since $d\sigma_{\gamma\gamma}^{(\text{fin.})}$ does not contain large logarithmic terms in the small- q_T region, it can be evaluated by truncation of the perturbative series at a given fixed order. The finite component is computed starting from the usual fixed-order perturbative truncation of the partonic cross section and subtracting the expansion of the resummed part at the same perturbative order. Introducing the subscript f.o. to denote the perturbative truncation of the various terms, we have:

$$\left[\frac{d\hat{\sigma}_{\gamma\gamma ab}^{(\text{fin.})}}{dq_T^2} \right]_{\text{f.o.}} = \left[\frac{d\hat{\sigma}_{\gamma\gamma ab}}{dq_T^2} \right]_{\text{f.o.}} - \left[\frac{d\hat{\sigma}_{\gamma\gamma ab}^{(\text{res.})}}{dq_T^2} \right]_{\text{f.o.}}. \quad (10)$$

This matching procedure between resummed and finite contributions guarantees to achieve uniform theoretical accuracy over the region from small to intermediate values of transverse momenta. At large values of q_T , the resummation (and matching) procedure is eventually superseded by the customary fixed-order calculations (their theoretical accuracy in the large- q_T region cannot be improved by resummation of the logarithmic terms that dominate in the small- q_T region).

As a summary of our presentation of the transverse momentum resummation formalism we can write that the inclusion of the functions $g^{(1)}$, $g_{N_1 N_2}^{(2)}$, $\mathcal{H}_{N_1 N_2}^{\gamma\gamma(1)}$ in the resummed component, together with the evaluation of the finite component at LO (i.e. at $\mathcal{O}(\alpha_s)$), allows us to perform the resummation at NLL+LO accuracy. This is the theoretical accuracy used in previous studies

[16, 63, 64, 65] of the diphoton q_T distribution. If we include also the functions $g_{N_1 N_2}^{(3)}$ and $\mathcal{H}_{N_1 N_2}^{\gamma\gamma(2)}$, together with the finite component at NLO (i.e. at $\mathcal{O}(\alpha_S^2)$) we can perform calculations at full NNLL+NLO accuracy.

In our particular case, using the $\mathcal{H}_{N_1 N_2}^{\gamma\gamma(2)}$ coefficient [21, 38], we are thus able to present the complete result for the diphoton q_T -distribution up to NNLL+NLO accuracy. The NNLL+NLO (NLL+LO) result includes the *full* NNLO (NLO) perturbative contribution in the small- q_T region. In particular, the NNLO (NLO) result for the total cross section is exactly recovered upon integration over q_T of the differential cross section $d\sigma_{\gamma\gamma}/dq_T$ at NNLL+NLO (NLL+LO) accuracy.

It is known that at small values of q_T , the perturbative QCD approach has to be supplemented with non-perturbative contributions, since they become relevant as q_T decreases. A discussion on non-perturbative effects on the q_T distribution is presented in Ref. [39, 56], and related quantitative results are shown in Sect. 3.

3. Numerical results for photon pair production at the LHC

We are interested in this section in the diphoton production in pp collisions at LHC energies ($\sqrt{s} = 7$ TeV). We present our resummed results at NNLL+NLO accuracy, and compare them with NLL+LO predictions and with available LHC data [6]. The formulation of the q_T resummation formalism that we use here is restricted to the production of colourless systems⁴ F , therefore it does not treat parton fragmentation subprocesses (here F includes one or two coloured partons that fragment); for this reason, we concentrate on the direct production of diphotons, and we rely on the smooth cone isolation criterion proposed by Frixione [57] (see also Ref. [67, 68]) which is defined by requesting

$$\sum E_T^{had} \leq E_{Tmax} \chi(r) ,$$

$$\text{inside any } r^2 = (y - y_\gamma)^2 + (\phi - \phi_\gamma)^2 \leq R^2 , \quad (11)$$

with a suitable choice for the function $\chi(r)$. This function has to vanish smoothly when its argument goes to zero ($\chi(r) \rightarrow 0$, if $r \rightarrow 0$), and it has to verify $0 < \chi(r) < 1$, if $0 < r < R$. One possible choice is

$$\chi(r) = \left(\frac{1 - \cos(r)}{1 - \cos R} \right)^n , \quad (12)$$

where n is typically chosen as $n = 1$. This condition implies that, closer to the photon, less hadronic activity is allowed inside the cone. When the parton and the photon are exactly collinear (at $r = 0$), the energy deposited inside the cone is required to be exactly equal to zero, and the fragmentation component (which is a purely collinear phenomenon in perturbative QCD) vanishes completely.

The cancellation of soft gluon effects takes place as in ordinary infrared-safe cross sections, since no region of the phase space is forbidden. That is the main advantage of this criterion: it eliminates all the fragmentation component in an infrared-safe way. By contrast, it can not be implemented within the usual experimental conditions; the standard way of implementing isolation in experiments is to use the prescription of Eq. (12) with a constant $\chi(r) = 1$. In any case, from a purely pragmatic point of view, it has been recently shown [58] that if the isolation parameters are tight enough (e.g., $E_{Tmax} < 6$ GeV, $R = 0.4$), the standard and the smooth cone isolation prescription coincide at the 1% level, which is well within the theoretical uncertainty of our predictions.

⁴ Transverse-momentum resummation for strongly-interacting final states, such as heavy-quark production, has been developed in Refs. [59, 60]. The first implementation of the q_T subtraction formalism was recently presented for top quark production at hadron colliders [66].

The acceptance criteria used in this analysis ($\sqrt{s} = 7$ TeV) are those implemented by the ATLAS collaboration analysis [6]; in all the numerical results presented in this proceeding, we require $p_T^{\text{harder}} \geq 25$ GeV, $p_T^{\text{softer}} \geq 22$ GeV, and we restrict the rapidity of both photons to satisfy $|y_\gamma| < 1.37$ and $1.52 < |y_\gamma| \leq 2.37$. The isolation parameters are set to the values $E_{T \text{ max}} = 4$ GeV, $n = 1$ and $R = 0.4$, and the minimum angular separation between the two photons is $R_{\gamma\gamma} = 0.4$. We use the Martin-Stirling-Thorne-Watt (MSTW) 2008 [69] sets of parton distributions, with densities and α_S evaluated at each corresponding order (i.e., we use $(n+1)$ -loop α_S at $N^n\text{LO}$, with $n = 0, 1, 2$), and we consider $N_f = 5$ massless quarks/antiquarks and gluons in the initial state. The default renormalization (μ_R) and factorization (μ_F) scales are set to the value of the invariant mass of the diphoton system, $\mu_R = \mu_F = M_{\gamma\gamma}$, while the default resummation scale (μ_{res}) is set to $\mu_{res} = M_{\gamma\gamma}/2$. The QED coupling constant α is fixed to $\alpha = 1/137$.

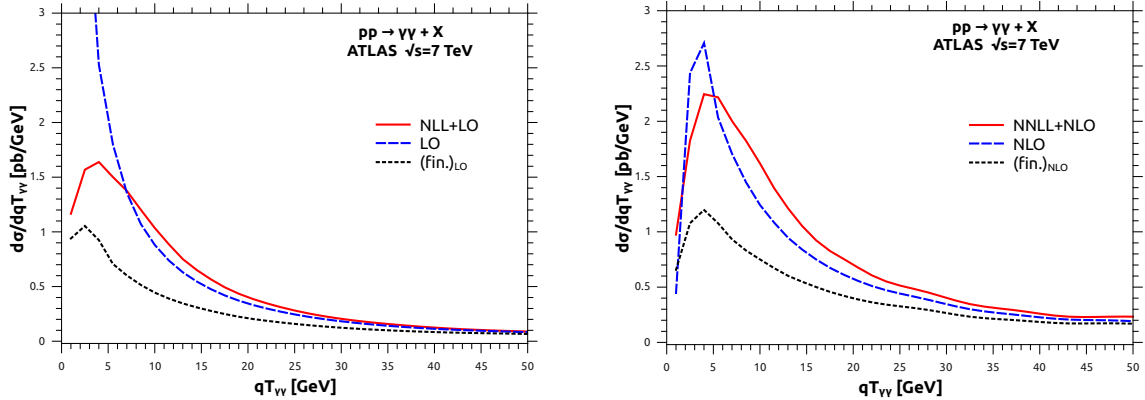


Figure 1. The q_T spectrum of the photon pair (solid red lines) at the LHC (7 TeV): results at NLL+LO (left panel) and NNLL+NLO (right panel) accuracy. Each result is compared to the corresponding fixed-order result (dashed lines) and to the finite component (dotted lines) in Eq. (10). The resummed spectrum includes a non-perturbative (NP) contribution parametrized as in Eq. (13).

Non-perturbative (NP) effects are expected to be important at very small q_T . Here we follow the strategy of Ref. [39], implementing them by multiplying the b -space form factor $\mathcal{W}^{\gamma\gamma}$ of Eq. (4) by a ‘NP factor’ which consists of a gaussian smearing of the form

$$S_{NP}^a = \exp(-C_a g_{NP} b^2), \quad (13)$$

where a denotes the initial state channel, $a = F$ for $q\bar{q}$ and $a = A$ for gg (as usual, $C_F = (N_c^2 - 1)/(2N_c)$ and $C_A = N_c$). In order to assess the importance of the NP contributions, in the Ref. [56] we varied g_{NP} in the interval from $g_{NP} = 0$ GeV² (no NP contributions) to $g_{NP} = 2$ GeV², corresponding to *moderate* NP effects [39]. As was shown in Ref. [56] the NP parameter that shows the better agreement with the data is $g_{NP} = 2$ GeV², therefore, in the rest of the proceeding we use this value to present all our results.

In Fig. 1, left panel, we present the NLL+LO q_T spectrum at the LHC ($\sqrt{s} = 7$ TeV). The NLL+LO result (solid line) at the default scales ($\mu_F = \mu_R = M_{\gamma\gamma}$; $\mu_{res} = M_{\gamma\gamma}/2$) is compared with the corresponding LO result (dashed line). The LO finite component of the spectrum (see Eq. (3)), is also shown for comparison (dotted line). We observe that the LO result diverges to $+\infty$ as $q_T \rightarrow 0$, as expected. The finite component is regular over the full q_T range, it

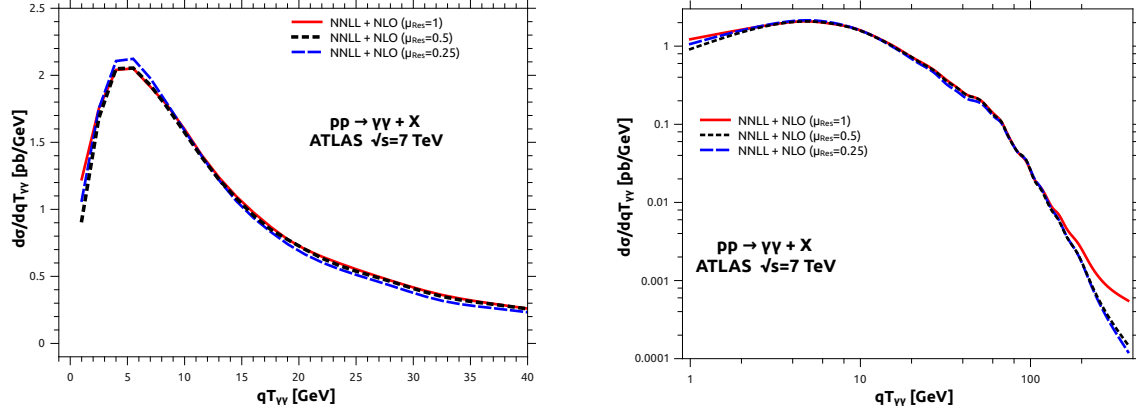


Figure 2. The q_T spectrum of diphoton production at the LHC ($\sqrt{s} = 7$ TeV). Here, the scales $\mu_F = \mu_R = M_{\gamma\gamma}$ are kept fixed while we vary the resummation scale μ_{res} to establish its impact on the cross section. In the left panel we show the range $0 \text{ GeV} < q_{T\gamma\gamma} < 40 \text{ GeV}$, and in the right panel the full spectra in logarithmic scale.

smoothly vanishes as $q_T \rightarrow 0$ and gives an important contribution to the NLL+LO result in the low- q_T region. That is mostly originated by the qg channel, which starts at NLO and provides a *subleading* correction in terms of logs (single logarithmic terms) but contributes considerably to the cross-section due to the huge partonic luminosity compared to the formally leading $q\bar{q}$ channel. The resummation of the small- q_T logarithms leads to a well-behaved distribution: it vanishes as $q_T \rightarrow 0$ and approaches the corresponding LO result at large values of q_T .

The results in the right panel of Fig. 1 are systematically at one order higher: the q_T spectrum at NNLL+NLO accuracy (solid line) is compared with the NLO result (dashed line) and with the NLO finite component of the spectrum (dotted line). The NLO result diverges to $-\infty$ as $q_T \rightarrow 0$ and, at small values of q_T , it has an unphysical peak that is produced by the compensation of negative leading and positive subleading logarithmic contributions. The contribution of the NLO finite component to the NNLL+NLO result is of the order of the 50% at the peak and becomes more important as q_T increases. A similar quantitative behaviour is observed by considering the contribution of the NLO finite component to the NLO result. At large values of q_T the contribution of the NLO finite component tends to the NLO result. This behaviour indicates that the logarithmic terms are no longer dominant and that the resummed calculation cannot improve upon the predictivity of the fixed-order expansion. We also observe that the position of the peak in the NNLL+NLO q_T distribution is slightly harder than the corresponding NLL+LO q_T distribution. This effect is (in part) due to the large transverse-momentum dependence of the fixed order corrections.

The resummed calculation depends on the factorization and renormalization scales and on the resummation scale μ_{res} , as discussed in Sect. 2. Our convention to compute factorization and renormalization scale uncertainties is to consider independent variations of μ_F and μ_R by a factor of two around the central values $\mu_F = \mu_R = M_{\gamma\gamma}$ in independent way in order to maximise them: $(\mu_F = 2 M_{\gamma\gamma}, \mu_R = M_{\gamma\gamma}/2, \mu_{res} = M_{\gamma\gamma}/2)$ and $(\mu_R = 2 M_{\gamma\gamma}, \mu_F = M_{\gamma\gamma}/2, \mu_{res} = M_{\gamma\gamma}/2)$. The uncertainty due to the resummation scale variation is assessed separately by varying it between $\mu_{res} = M_{\gamma\gamma}/4$ and $\mu_{res} = M_{\gamma\gamma}$ at fixed μ_F and μ_R .

In order to estimate the impact of the resummation scale μ_{res} , we show in Fig. 2 the NNLL+NLO transverse momentum distribution for three different implementations of the μ_{res} parameter ($\mu_{res} = M_{\gamma\gamma}/4; M_{\gamma\gamma}/2; M_{\gamma\gamma}$) at fixed $\mu_F = \mu_R = M_{\gamma\gamma}$. The impact of the variation

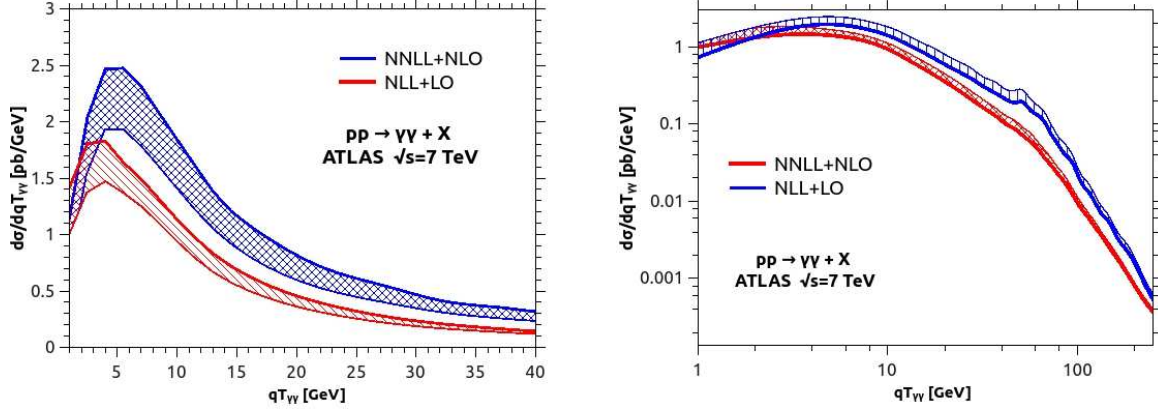


Figure 3. The q_T spectrum of diphoton pairs at the LHC. The NNLL+NLO result is compared with the NLL+LO result, for the window $0 \text{ GeV} < q_T < 40 \text{ GeV}$ (left panel) and the full spectra (right panel). The bands are obtained by varying μ_R and μ_F as explained in the text.

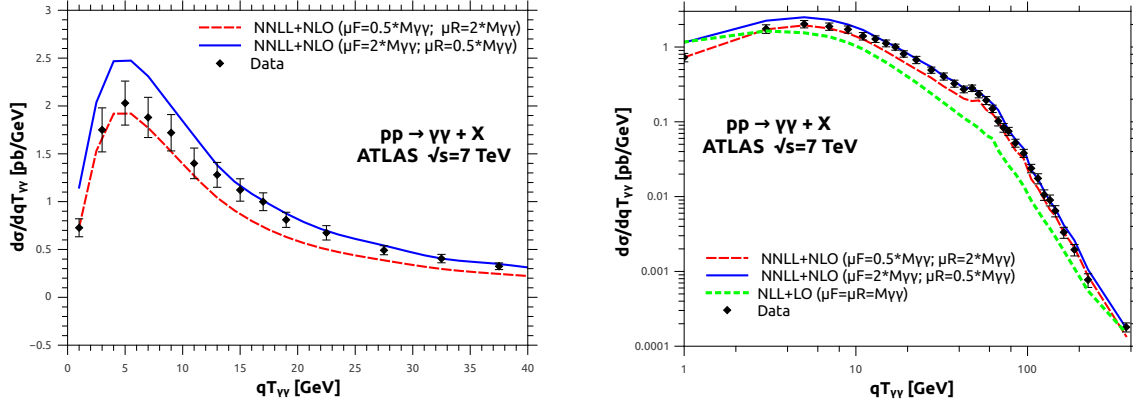


Figure 4. Comparison of the theoretical prediction for the q_T spectrum of diphoton pairs at the LHC with the experimental data. The NNLL+NLO result is compared with the ATLAS data of Ref. [6], for the window $0 \text{ GeV} < q_T < 40 \text{ GeV}$ (left panel) and the full spectra (right panel). In the right panel the NLL+LO distribution at central scale (dotted line) is also shown in order to compare it with the data and the NNLL+NLO result. The bands (solid and dashed lines) are obtained by varying μ_R and μ_F as explained in the text.

of the μ_{res} scale in the cross section is at per-cent level. In the left panel of Fig. 2 we present the transverse momentum distribution for values of q_T within the interval $0 \text{ GeV} < q_T < 40 \text{ GeV}$, and in the right panel of Fig. 2 the full spectra. We also notice that the strongest effect of the variation of the μ_{res} scale appears in the last bin of right panel of Fig. 2. This is expected since the resummation scale effectively *sets* the value of transverse momentum at which the logarithms are dominant. A choice of a very large resummation scale affects the distribution at larger transverse momentum and might in general result in a mismatch with the fixed order prediction due to the artificial introduction of unphysically large logarithmic contributions in that region.

In Fig. 3 we compare the variation of the scales of the NNLL+NLO and NLL+LO predictions,

for the interval $0 \text{ GeV} < q_T < 40 \text{ GeV}$ (left panel) and the full spectra (right panel). As in the case of the fixed order calculation [21], the dependence on the scales is not reduced when going from NLL+LO to NNLL+NLO. This is mostly because at NNLL+NLO a new channel (gg) opens, in which the box contribution (effectively “LO” but formally $\mathcal{O}(\alpha_S^2)$) ruins the reduction of the scale dependence usually expected when adding second order corrections for the $q\bar{q}$ channel and first order corrections for the qg channel. Since NNLL+NLO is the first order at which all partonic channels contribute, it is possible to argue that this is the first order at which estimates of theoretical uncertainties through scale variations can be considered as reliable.

In the right panel of Fig. 3 we observe the so called *Guillet shoulder* [70], which is a real radiation effect and has its origin in the fixed order contribution. It appears stronger in the NNLL+NLO q_T distribution than in the NLL+LO, due to the larger size of the real contributions at NLO.

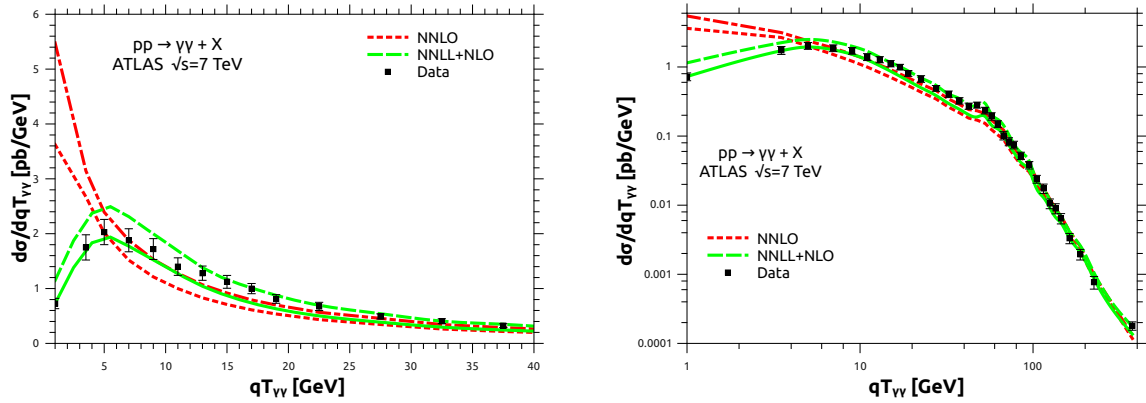


Figure 5. Comparison of the theoretical prediction for the q_T spectrum of diphoton pairs at the LHC with the experimental data. The NNLL+NLO result (green dashed band) and the fixed order result at NLO (red dotted band) are compared with the ATLAS data of Ref. [6], for the window $0 \text{ GeV} < q_T < 40 \text{ GeV}$ (left panel) and the full spectra (right panel). The bands (dotted and dashed lines) are obtained by varying μ_R and μ_F as explained in the text.

In Fig. 4 we compare the LHC data ($\sqrt{s} = 7 \text{ TeV}$) from ATLAS [6] with our resummed theoretical predictions (at NNLL+NLO and NLL+LO). We estimate the theoretical uncertainty by the variation of the μ_R and μ_F scales. In the left panel we show the q_T distribution in the window ($0 \text{ GeV} < q_T < 40 \text{ GeV}$), while in the right ones we show the full spectra in logarithmic scale.

We observe in general an excellent agreement between the resummed NNLL+NLO prediction and the experimental data, that is accurately described within the theoretical uncertainty bands in the whole kinematic range. Also we note that the NLL+LO result is not enough to describe the phenomenology of the transverse-momentum distribution of the LHC data (Fig. 4, right panel). By direct comparison to the fixed order prediction, we notice that the effect of resummation is not only to recover the predictivity of the calculation at small transverse momentum, but also to improve substantially the agreement with LHC data [6].

In order to understand how the resummed result improves the fixed order theoretical description of the data, we present in Fig. 5 the comparison of the theoretical prediction for the q_T spectrum of diphoton pairs at the LHC with the experimental data. The NNLL+NLO result (green dashed band) and the fixed order result at NLO (red dotted band) are compared with the ATLAS data of Ref. [6], for the window $0 \text{ GeV} < q_T < 40 \text{ GeV}$ (left panel) and the full

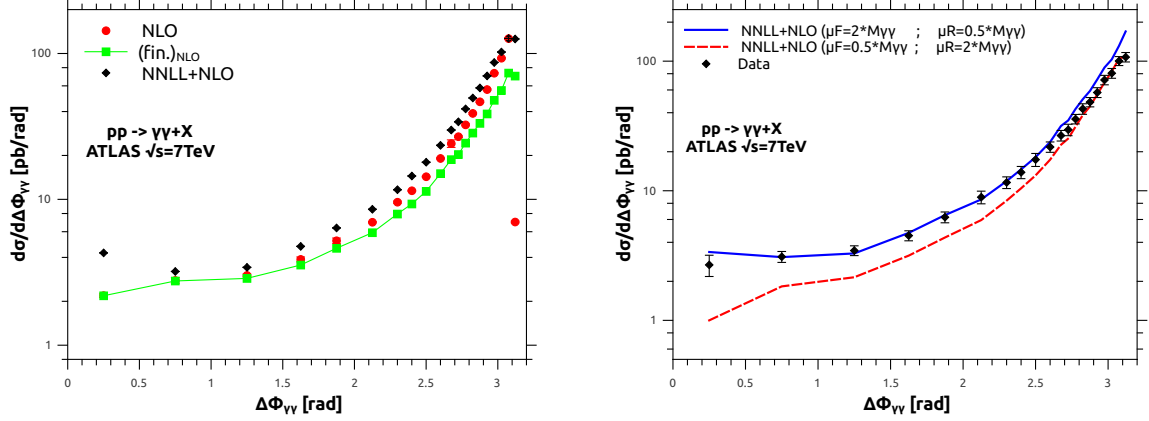


Figure 6. The $\Delta\Phi_{\gamma\gamma}$ distribution of diphoton pairs at the LHC. In the left panel, we show the fixed order prediction, the complete resummed prediction and just the resummed contribution at the central scale. In the right, the full NNLL+NLO result (using the extreme values for μ_R and μ_F to estimate the theoretical uncertainty) is compared with the ATLAS data of Ref. [6].

spectra (right panel). Two comments are in order: i) in the small- q_T region ($q_T \ll M_{\gamma\gamma}$) where the prediction of the fixed order result is not reliable, we observe how the resummed distribution improves the description of the phenomenology of the data; ii) in the large- q_T region ($q_T \sim M_{\gamma\gamma}$) where the effects of resummation vanish, the resummed distribution tends to fixed order result, as expected.

While the resummation performed in this work reaches NNLL accuracy formally only for the diphoton transverse momentum distribution, its predictions can be extended to other observables as well, since at least the leading logarithmic contributions have a common origin from soft and collinear emission.

In Fig. 6 we present the results of the cross section as a function of the azimuthal angle $\Delta\Phi_{\gamma\gamma}$. In the left panel we compare the fixed order (NLO), finite (NLO) and full (NNLL+NLO) $\Delta\Phi_{\gamma\gamma}$ distributions. The fixed order component dominates the cross section over the whole $\Delta\Phi_{\gamma\gamma}$ range. However, as could be expected, the effect of resummation is stronger for kinematic configurations near the $\Delta\Phi_{\gamma\gamma} \sim \pi$ which correspond to $q_T \sim 0$ GeV. As in the case of the fixed order q_T distribution, the $\Delta\Phi_{\gamma\gamma}$ fixed order differential cross section is not well-behaved near the back-to-back configuration: it actually diverges as $\Delta\Phi_{\gamma\gamma} \rightarrow \pi$ ($q_T \rightarrow 0$). The finite contribution (Eq. (10)) is well-behaved near the back-to-back configuration, and the full result (NNLL+NLO) improves the description in the region near $\Delta\Phi_{\gamma\gamma} \sim 0$. In the right panel of Fig. 6 we compare our theoretical prediction at NNLL+NLO level of accuracy (using the variation of the μ_R and μ_F scales to estimate the theoretical uncertainty) with the LHC data [6]. We observe that the transverse momentum resummation provides a better description of the data with respect to the fixed order result.

4. Summary

We presented the transverse momentum resummation for photon pair production at NNLL accuracy in hadron collisions. In the small q_T region, we included the resummation of all logarithmically-enhanced perturbative QCD contributions, up to next-to-next-to-leading logarithmic accuracy; at intermediate and large values of q_T , we combined the resummation with the fixed next-to-leading order perturbative result. The matching between the fixed-order

and the resummed results is performed in such a way as to exactly reproduce the known next-to-next-to-leading order result for the total cross section; in the end, the calculation consistently includes all perturbative terms up to formal order α_S^2 . The theoretical uncertainty was estimated by varying the various scales (renormalization, factorization and resummation) introduced by the formalism. Our results were compared to experimental data, showing good agreement between theory and experiment over the whole q_T range. With respect to the fixed-order calculation, the present implementation provides a better description of the data and recovers the correct physical behaviour in the small q_T region, with the spectrum smoothly going to zero. The same set-up also allows the calculation of more exclusive observable distributions; the $\Delta\Phi_{\gamma\gamma}$ distribution is a given example.

References

- [1] S. Chatrchyan *et al.* [CMS Collaboration], JHEP **1201** (2012) 133
- [2] T. Aaltonen *et al.* [CDF Collaboration], Phys. Rev. D **84** (2011) 052006
- [3] S. Chatrchyan *et al.* [CMS Collaboration], Eur. Phys. J. C **74** (2014) 11, 3129
- [4] V. M. Abazov *et al.* [D0 Collaboration], Phys. Lett. B **725** (2013) 6
- [5] G. Aad *et al.* [ATLAS Collaboration], Phys. Rev. D **85** (2012) 012003.
- [6] G. Aad *et al.* [ATLAS Collaboration], JHEP **1301** (2013) 086
- [7] S. Chatrchyan *et al.* [CMS Collaboration], Phys. Lett. B **716** (2013) 30
- [8] G. Aad *et al.* [ATLAS Collaboration], Phys. Lett. B **716** (2013) 1
- [9] **ATLAS** Collaboration, G. Aad *et al.*, , *Phys.Lett.* **B718** (2012) 411–430,
- [10] S. Chatrchyan *et al.* [CMS Collaboration], JHEP **1303** (2013) 111
- [11] G. Aad *et al.* [ATLAS Collaboration], New J. Phys. **15** (2013) 043007
- [12] **CMS** Collaboration, S. Chatrchyan *et al.*, , *Phys. Lett. B.* (2012)
- [13] T. Binoth *et al.* Eur. Phys. J. **C16**, 311 (2000).
- [14] Z. Bern, L. J. Dixon and C. Schmidt, Phys. Rev. **D66**, 074018 (2002).
- [15] J. M. Campbell, R. K. Ellis and C. Williams, JHEP **1107**, 018 (2011).
- [16] C. Balazs, E. L. Berger, P. M. Nadolsky and C. -P. Yuan, Phys. Rev. **D76**, 013009 (2007).
- [17] D. A. Dicus and S. S. D. Willenbrock, Phys. Rev. **D37**, 1801 (1988).
- [18] V. D. Barger, *et al.*, Phys. Rev. **D41**, 2782 (1990); V. Del Duca, *et al.* Nucl. Phys. **B566**, 252 (2000).
- [19] Z. Bern, *et al.*, Nucl. Phys. **B437**, 259 (1995); A. Signer, Phys. Lett. **B357**, 204 (1995).
- [20] C. Anastasiou, E. W. N. Glover and M. E. Tejeda-Yeomans, Nucl. Phys. **B629**, 255 (2002).
- [21] S. Catani, *et al.*, Phys. Rev. Lett. **108** (2012) 072001
- [22] V. Del Duca, F. Maltoni, Z. Nagy and Z. Trocsanyi, JHEP **0304**, 059 (2003).
- [23] T. Gehrmann, N. Greiner and G. Heinrich, JHEP **1306** (2013) 058 [Erratum-ibid. **1406** (2014) 076]
- [24] Z. Bern, L. J. Dixon, F. Febres Cordero, S. Hoeche, H. Ita, D. A. Kosower, N. A. Lo Presti and D. Maitre, Phys. Rev. D **90** (2014) 5, 054004
- [25] T. Gehrmann, N. Greiner and G. Heinrich, Phys. Rev. Lett. **111** (2013) 222002
- [26] S. Badger, A. Guffanti and V. Yundin, JHEP **1403** (2014) 122
- [27] Y. L. Dokshitzer, D. Diakonov and S. I. Troian, Phys. Lett. B **79** (1978) 269, Phys. Rep. **58** (1980) 269.
- [28] G. Parisi and R. Petronzio, Nucl. Phys. B **154** (1979) 427.
- [29] G. Curci, M. Greco and Y. Srivastava, Nucl. Phys. B **159** (1979) 451.
- [30] J. C. Collins and D. E. Soper, Nucl. Phys. B **193** (1981) 381 [Erratum-ibid. B **213** (1983) 545].
- [31] J. C. Collins and D. E. Soper, Nucl. Phys. B **197** (1982) 446.
- [32] J. Kodaira and L. Trentadue, Phys. Lett. B **112** (1982) 66, report SLAC-PUB-2934 (1982), Phys. Lett. B **123** (1983) 335.
- [33] C. T. H. Davies and W. J. Stirling, Nucl. Phys. B **244** (1984) 337.
- [34] C. T. H. Davies, B. R. Webber and W. J. Stirling, Nucl. Phys. B **256** (1985) 413.
- [35] G. Altarelli, R. K. Ellis, M. Greco and G. Martinelli, Nucl. Phys. B **246** (1984) 12.
- [36] J. C. Collins, D. E. Soper and G. Sterman, Nucl. Phys. B **250** (1985) 199.
- [37] S. Catani, D. de Florian and M. Grazzini, Nucl. Phys. B **596** (2001) 299.
- [38] S. Catani, L. Cieri, D. de Florian, G. Ferrera and M. Grazzini, Nucl. Phys. B **881** (2014) 414
- [39] G. Bozzi, S. Catani, D. de Florian and M. Grazzini, Nucl. Phys. B **737** (2006) 73.
- [40] G. Bozzi, S. Catani, D. de Florian and M. Grazzini, Nucl. Phys. B **791** (2008) 1.
- [41] S. Catani and M. Grazzini, Nucl. Phys. B **845** (2011) 297 [arXiv:1011.3918 [hep-ph]].
- [42] G. Bozzi, S. Catani, D. de Florian and M. Grazzini, Phys. Lett. B **564** (2003) 65.
- [43] D. de Florian, G. Ferrera, M. Grazzini and D. Tommasini, JHEP **1111** (2011) 064

- [44] D. de Florian, G. Ferrera, M. Grazzini and D. Tommasini, JHEP **1206** (2012) 132
- [45] R. V. Harlander, A. Tripathi and M. Wiesemann, Phys. Rev. D **90** (2014) 1, 015017
- [46] R. V. Harlander, H. Mantler and M. Wiesemann, JHEP **1411** (2014) 116
- [47] G. Bozzi, S. Catani, G. Ferrera, D. de Florian and M. Grazzini, Nucl. Phys. B **815** (2009) 174.
- [48] G. Bozzi, S. Catani, G. Ferrera, D. de Florian and M. Grazzini, Phys. Lett. B **696** (2011) 207
- [49] S. Catani, D. de Florian, G. Ferrera and M. Grazzini,
- [50] M. Grazzini, JHEP **0601** (2006) 095.
- [51] P. Meade, H. Ramani and M. Zeng, Phys. Rev. D **90** (2014) 11, 114006
- [52] R. Frederix and M. Grazzini, Phys. Lett. B **662** (2008) 353.
- [53] M. Grazzini, S. Kallweit, D. Rathlev and M. Wiesemann, JHEP **1508** (2015) 154
- [54] G. Bozzi, B. Fuks and M. Klasen, Phys. Rev. D **74** (2006) 015001.
- [55] H. Kawamura, J. Kodaira, H. Shimizu and K. Tanaka, Prog. Theor. Phys. **115** (2006) 667; H. Kawamura, J. Kodaira and K. Tanaka, Nucl. Phys. B **777** (2007) 203, Prog. Theor. Phys. **118** (2007) 581, Phys. Lett. B **662** (2008) 139.
- [56] L. Cieri, F. Coradeschi and D. de Florian, JHEP **1506** (2015) 185
- [57] S. Frixione, Phys. Lett. B **429** (1998) 369
- [58] J. Butterworth, G. Dissertori, S. Dittmaier, D. de Florian, N. Glover, K. Hamilton, J. Huston and M. Kado *et al.*,
- [59] H. T. Li, C. S. Li, D. Y. Shao, L. L. Yang and H. X. Zhu, Phys. Rev. D **88** (2013) 074004
- [60] S. Catani, M. Grazzini and A. Torre, Nucl. Phys. B **890** (2014) 518
- [61] D. de Florian and M. Grazzini, Phys. Rev. Lett. **85** (2000) 4678, Nucl. Phys. B **616** (2001) 247.
- [62] T. Becher and M. Neubert, Eur. Phys. J. C **71** (2011) 1665
- [63] C. Balazs, E. L. Berger, P. M. Nadolsky and C.-P. Yuan, Phys. Lett. B **637** (2006) 235
- [64] P. M. Nadolsky and C. R. Schmidt, Phys. Lett. B **558** (2003) 63
- [65] C. Balazs, P. M. Nadolsky, C. Schmidt and C. P. Yuan, Phys. Lett. B **489** (2000) 157
- [66] R. Bonciani, S. Catani, M. Grazzini, H. Sargsyan and A. Torre, arXiv:1508.03585 [hep-ph].
- [67] S. Frixione and W. Vogelsang, Nucl. Phys. B **568** (2000) 60
- [68] S. Catani, M. Dittmar, D. E. Soper, W. J. Stirling, S. Tapprogge, S. Alekhin, P. Aurenche and C. Balazs *et al.*, In *Geneva 1999, Standard model physics (and more) at the LHC* 1-115
- [69] A. D. Martin, W. J. Stirling, R. S. Thorne and G. Watt, Eur. Phys. J. C **63** (2009) 189.
- [70] T. Binoth, J. P. Guillet, E. Pilon and M. Werlen, Phys. Rev. D **63** (2001) 114016